Experimental Thermal and Fluid Science 84 (2017) 165–178

Contents lists available at ScienceDirect

Experimental Thermal and Fluid Science

journal homepage: www.elsevier.com/locate/etfs

Analysis and comparison of internal and external temperature measurements of a tubular oscillating heat pipe

J. Gabriel Monroe [a], Zachary S. Aspin [b], John D. Fairley [c], Scott M. Thompson [d,*]

[a] Engineer Research and Development Center (ERDC), US Army Corps of Engineers, Vicksburg, MS 39180, USA
[b] Commercial and Industrial Solutions (CIS), Grenada, MS 38901, USA
[c] Sandia National Laboratories, Albuquerque, NM 87123, USA
[d] Laboratory for Fatigue & Additive Manufacturing Excellence (FAME), Department of Mechanical Engineering, Auburn University, Auburn, AL 36849, USA

ARTICLE INFO

Article history:
Received 6 September 2016
Received in revised form 20 January 2017
Accepted 29 January 2017
Available online 9 February 2017

Keywords:
Oscillating heat pipe
Pulsating heat pipe
Heat transfer coefficient
Tubular conduction
Frequency analysis
Fluid pulsation

ABSTRACT

The current study examines the relationship between internal/fluidic and external/wall temperature measurements along the adiabatic section of an operating tubular oscillating heat pipe (T-OHP) for varying heat inputs. Temperature measurements were achieved using type-T thermocouples located either inside or along the OHP wall in the region between the evaporator and condenser. Measurements were utilized to elucidate the effects of wall thermal capacitance, external wall temperature gradient, and internal fluid advection. The internal, single-phase heat transfer coefficient was estimated, and the effective thermal conductivity of the OHP was determined. A 4-turn copper T-OHP (3.25 mm ID) was charged with water (75% by volume) and tested in the bottom-heating condition. Heat input was varied in increments of 25 W from 60 W to 300 W. Results indicate that the external thermocouples were unable to capture frequency components larger than ~1 Hz. Internal measurements indicate that average, evaporator-side fluid oscillation frequencies varied from ~1.5 Hz at 60 W to ~2.5 Hz at 300 W, whereas condenser-side frequencies remained fairly constant at ~0.5 Hz. The frequency transfer function corresponding to the thermal resistance network between the internal/external thermocouples was found to be constant across all tested power inputs. The low-frequency, large-amplitude changes in internal temperature associated with bulk fluid motion were not immediately measured at the external OHP tube surface. The effective thermal conductivity calculated using only external temperature measurements was found to be 4–12% lower than that calculated using internal measurements. The maximum, calculated effective thermal conductivity using internal or external temperature measurements was 15,300 W/m·K and 14,000 W/m·K, respectively. This difference arises from there being a smaller, length-wise temperature gradient along the fluid columns than along the tube wall due to the strong advection component of OHP heat transfer. Tube wall conduction was found to account for 2–10% of the overall heat transfer, with its significance decreasing as fluid advection increased at higher heat inputs. The heat transfer coefficient for single-phase fluid oscillation inside the OHP was estimated to be ~1000 W/m^2 K for power inputs larger than 100 W; corresponding to Nusselt numbers between 4 and 6.

1. Introduction

Oscillating heat pipes (OHPs), also referred to as pulsating heat pipes (PHPs), have been actively investigated since their inception in the early 1990s [1] due, in part, to their relatively high manufacturability and heat transfer ability. The OHP is a two-phase heat transfer device that relies on pressure driven fluid oscillations within a hermetically-sealed capillary structure that is partially filled with working fluid at negative pressure. As shown in Fig. 1, the OHP can exist as either a closed-loop, serpentine-arranged capillary tube for axial-wise heat transfer, *i.e.* a tubular OHP (T-OHP), or as meandering mini- or micro-channels embedded in solid media for axial or spreading heat transfer, *i.e.* a flat-plate OHP (FP-OHP). The T-OHP is relatively easy to manufacture and lends itself for heat transfer in low-flux operating environments; for applications such as waste heat recovery or energy harvesting [2–7], while FP-OHPs can be more readily miniaturized for high heat flux applications (*e.g.* electronics cooling) because of their high channel density relative to T-OHPs [8–12]. As shown in Fig. 1, the axial heat transfer mode of the OHP consists of

* Corresponding author at: Department of Mechanical Engineering, Auburn University, 354 War Eagle Way, Auburn, AL 36849, USA.
E-mail address: scott.thompson@auburn.edu (S.M. Thompson).

http://dx.doi.org/10.1016/j.expthermflusci.2017.01.020
0894-1777/

Nomenclature

$A_{c,w}$	cross-sectional area of OHP tube wall, m^2
d	counting index
d_{in}	inner diameter, mm
d_h	hydraulic diameter, mm
d_o	outer diameter, mm
f	frequency, Hz
$\bar{f}$	spatial average of local mean oscillation frequencies, Hz
g	acceleration due to gravity, m/s^2
h	heat transfer coefficient, $W/m^2 \cdot K$
$\hat{h}$	specific enthalpy, J/kg
H	frequency transfer function
ID	inner diameter, mm
j	$\sqrt{-1}$
k	thermal conductivity, W/m·K
m	counting index
$\dot{m}$	mass flow rate, kg/s
n	counting index
N	length of a signal, or number of samples
OD	outer diameter
P	electrical power input, W
q	heat transfer, W
r	radius
R_{xy}	normalized cross correlation of signals x and y
S	amplitude spectrum of a zero-shifted temperature signal, Δ°C
T	temperature, °C
TC	thermocouple
x, y	zero-shifted temperature signals, Δ°C
X, Y	discrete Fourier transforms of zero-shifted temperature signals, Δ°C
z	spatial coordinate in axial direction along channels of the OHP, cm
Δz	axial distance between thermocouples, cm
Δ%	percent difference
Δt	sampling period, s
ΔT	temperature difference, °C

Greek symbols

α	thermal diffusivity, m^2/s
μ	dynamic viscosity, Pa·s
ρ	density, kg/m^3
ψ	thermal resistance, °C/W
σ	surface tension, N/m
τ	average time lag, s

Subscripts

adia	with respect to the T-OHP adiabatic section
cond	conduction
conv	convection
e	with respect to external temperature readings
eff	effective
i	with respect to internal temperature readings, or counting index
j	counting index
liq	liquid
n	counting index
vap	vapor
s	sampling
sp	single phase

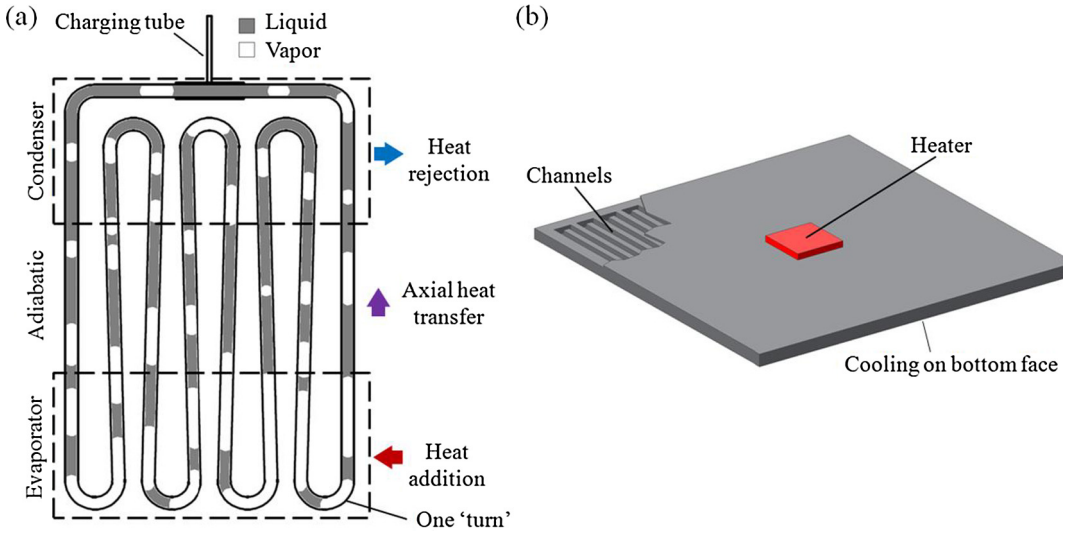

Fig. 1. (a) A bottom-heated, 4-turn T-OHP (transparent view) for axial heat transfer and (b) a FP-OHP operating as a heat spreader with internal channel structure shown.

well-defined regions along its geometry; the 'evaporator' and 'condenser' regions are where heat is added or rejected from the OHP, respectively, while the 'adiabatic' region is where heat is transferred almost exclusively along the length of the OHP.

The initial two-phase fluid distribution within the OHP can be near-random. However, once the OHP is located within a sufficient thermal gradient and/or heat flux, the heat transfer through the OHP evaporator (region of heat input) overcomes the working fluid's latent heat of vaporization, and the encapsulated liquid begins to vaporize and expand (see Fig. 1). This 'start-up' phase of the OHP results in the internal, two-phase fluid distribution gradually shifting due to heat transfer and pressure imbalance.

When the temperature gradient and/or heat flux sufficiently exceeds that required for OHP start-up, the device can achieve pseudo steady-state operation due to cyclic vapor expansion in the evaporator and vapor contraction due to condensation in the condenser (region of heat rejection). Such steady-state OHP operation is typically characterized by the oscillatory locomotion of liquid between the evaporator and condenser. The start-up of an OHP can be inhibited due to many factors, including the conduction thermal resistance of its container and the inertance of the encapsulated working fluid. Start-up can be assisted by reducing channel/tube pressure losses, changing the working fluid, or imposing beneficial boundary conditions, *e.g.* ultrasonic sound for stimulating the encapsulated working fluid [13].

Presence of a transverse pressure gradient across the evaporator 'turns' is essential for sustaining the oscillating/pulsating flow of the entrapped two-phase fluid. Although the phase-change cycle drives OHP operation, latent heat transfer within the OHP typically only accounts for ~10% of the total heat transfer [14,15]. Instead, the majority of heat transfer is sensible and due to convection of the oscillating liquid/vapor distribution. The combination of sensible and latent heat transfer results in a highly efficient heat transfer process with relatively few operating limitations [16]. One known OHP operating limitation is 'dry-out', which occurs at relatively high heat inputs and/or evaporator temperatures [17]. This phenomenon is characterized by the cessation of fluid oscillation due to vapor over-expansion (or vapor 'lock'), pressure-balancing in the evaporator, and the subsequent lack of liquid vaporization and/or pumping in the evaporator.

During OHP operation, the internal fluid motion causes the OHP external surface temperature field to oscillate with respect to time. This dynamic temperature field is often utilized as a means to characterize OHP thermal performance. As an example, a reduced temperature difference between the evaporator and condenser, for the same heat flux, is an indicator of the OHP possessing a higher heat transfer capability; and an evaporator temperature that steadily increases with time and ceases to oscillate is indicative of OHP dry-out or pressure balancing throughout the channels. Both OHP start-up and dry-out are easily identified by a sudden decrease or increase in the effective thermal resistance of the OHP, respectively [17]. The OHP can operate in various orientations, heating/cooling configurations, and gravity conditions [18,19]. Working orientations can vary, for example, between bottom/vertical-, horizontal-, and top/vertical-wise heating. During bottom/vertical-wise heating, the evaporator is located below the condenser and the OHP is oriented normal to ground, as shown in Fig. 1(a).

Measuring the temperature distribution of an operating OHP provides the analytical/numerical modeler with valuable data for OHP model verification and validation. This is important since, to date, the existence of a widely-applicable, accurate OHP model is limited. Although this is mostly due to the many OHP design possibilities and complex thermal/fluid phenomena that occur during OHP operation [20], it can also be attributed to the difficulty of relating experimental measurement with actual physical phenomena. Hence, many researchers continue to rely on semi-empirical models and external surface temperature measurements via TCs to characterize OHP thermal performance.

Contact-type measurement devices, such as thermocouples (TCs), are a desirable means for measuring the OHP surface temperature field at local regions. Although TCs limit one to measuring a discrete temperature field (*i.e.* spatial samples of the overall surface temperature field), the temperature at specific locations can be collected at high frequency – with encumbered measurements often referred to as temperature signals or thermal oscillations. Infrared (IR) thermography provides a means to observe a more continuous OHP temperature field; however, many IR cameras possess lower temporal resolution relative to TCs. In addition, thermal characterization of OHPs often requires an OHP to be insulated from its surroundings to better quantify evaporator-to-condenser heat transfer. Utilization of insulating materials can obscure the visibility of the OHP's thermal footprint.

The TC junction is formed by spot welding the ends of the TC wires into a small bead; note that the bead size will affect how fast the TC responds to a temperature change. While there are many possible metal combinations for effective TCs, type-T (constantan/-copper) [11,21,22] and type-K (chromel/alumel) [6,23,24] are the most common combinations for measuring OHP surface temperature at temperatures $\lesssim 200\,^{\circ}C$. Mismatch in thermal conductivity, specific heat capacity, and density at a TC/material-surface junction can affect accuracy in transient temperature measurements [25]. In general, the specific heat capacity and density of a TC should be smaller than that of the measured material, while the TC thermal conductivity should be larger, *i.e.* the ratio of thermal diffusivities, α_{TC}/α_{mat}, should be as large as possible to maximize TC frequency response. Xue et al. also showed that poorly matched TC and material properties can result in 20 dB signal attenuation at frequencies under 1 Hz. In addition to TC design, TC response time can be affected by experiment and/or environmental factors, such as the nature of fluid flow, type of fluid and measured media geometry [26,27].

Temperature measurements obtained via OHP-attached TCs can be analyzed, for example, by frequency (*i.e.* Fourier, signal analysis) or statistical methods to obtain better insight into OHP operating behavior. Xu and Zhang [28] investigated thermal oscillations in a 3-turn, 18.0 cm long copper T-OHP at relatively low power inputs (10–25 W) using perfluorohexane as the working fluid at a filling ratio (volume of liquid to internal volume of OHP) of 70%. The OHP had a 2 mm ID (and 0.5 mm wall thickness) and was cooled by natural convection in air without an additional heat sink. Via power spectrum analysis of the external temperature measurements, it was observed that at lower heat inputs thermal oscillations were more random but still possessed a dominant frequency (~0.1 Hz). At higher heat inputs the temperature fluctuations were found to become quasi-periodic with a higher dominant frequency of ~0.5 Hz.

Thompson and Ma [29] used statistical methods to compare the measurable temperature field of two 6-turn, 13.6 cm long copper FP-OHPs. One FP-OHP had Tesla-type check valves (TV FP-OHP) installed in its adiabatic region (*i.e.* the insulated, middle OHP region; see Fig. 1) to promote passive flow control for heat transfer enhancement. All temperature measurements were taken along the external surface of each FP-OHP. The steady-state temperature signals were found to have multiple frequency components best modeled via a multi-modal Gaussian probability density function. Low frequency elements were attributed to temporary pauses, or stopovers, in fluid oscillation during OHP operation, since the TV FP-OHP exhibited fewer Gaussian mixture components than the un-valved FP-OHP. It was also found that temperature changes in the evaporator and condenser were closely linked for both OHPs investigated, as evident by Pearson correlation coefficients on-the-order of 0.7. Fairley et al. [12] applied time-frequency analysis techniques, such as the short-time Fourier transform and the Hilbert-Huang transform, to further characterize the externally-measured TV FP-OHP evaporator temperature signals. It was found that the temperature signals oscillated predominantly at sub-0.2 Hz frequencies and that these oscillations did not occur at a constant frequency during OHP operation, but instead behaved intermittently.

Suzuki [30] investigated the temperature fluctuations and effective thermal conductivity of a 4-turn, open-loop T-OHP. The T-OHP was 36.0 cm long and made from 2 mm ID, 3 mm OD copper tubing. Twenty-five TCs were attached to the outer wall surfaces along

the T-OHP's adiabatic region. Heat input was varied from 50 to 300 W, and it was generally observed that temperature signals oscillated at frequencies between 1 and 2 Hz. Fluid pressure can always be used to characterize OHP performance, as was shown by Kim et al. [31] who used 9 pressure sensors placed in the evaporator and condenser to investigate the effect of filling ratio, heat flux, and inclination angle on the pressure oscillations inside a 22.0 cm long FP-OHP. They used a 10-turn, 1.5 mm square channel, brass FP-OHP with a transparent acrylic cover plate. It was seen that, in general, the saturation pressure of the liquid (R-142b) increased as heat flux and charge ratio increased. At heat fluxes of 0.6–0.9 W/cm^2, the pressure frequency was seen to be ~1–2 Hz.

Zhang and Faghri [32] presented a numerical model for predicting the behavior of an open-loop OHP with an arbitrary numbers of turns. The model suggests that for six or less turns, the OHP performs uniformly with regard to temperature oscillation amplitude and frequency (*i.e.* the motion of the various liquid slugs stays in-phase). The opposite is seen for an OHP with six or more turns, in which the amplitude and frequency of temperature oscillations of liquid slugs in adjacent turns are more out-of-phase. In an attempt to create a practical model for assisting OHP design, Furukawa [33] expanded upon the work of Ma et al. [34,35] and derived closed-form algebraic expressions capable of predicting fluid oscillation frequency/amplitude and the temperature difference between the OHP evaporator and condenser. Predictions from the model were compared with the results from multiple experimental references with reasonable accuracy.

Mameli et al. [36] investigated the thermo-fluidic behavior within a two-turn, closed-loop T-OHP made from copper and acrylic tubing and quantified the local heat transfer coefficient within its evaporator and condenser. The lengths of the evaporator, condenser, and adiabatic sections were 25 mm, 35 mm, and 202 mm, respectively. The copper/acrylic T-OHP was filled with ethanol to a filling ratio of 65%, and a pressure probe was installed in the condenser. During operation, the condenser was cooled using water held at 15 °C via a thermal-controlled circulation bath. In order to directly measure local fluid temperature inside the T-OHP, type-K TCs (bead dimension 0.3 mm, accuracy ±0.2 °C) were installed into 1.0 mm diameter holes drilled through the tubing in each turn of the evaporator and sealed with high temperature-resistant thermal cement; six additional type-K TCs were also externally mounted to the tubing in the evaporator. The T-OHP was tested at power inputs ranging from 50 W to 100 W. The local heat transfer coefficient in the evaporator was found to increase with increasing input power, approaching an asymptotic value of approximately 4600 W/m^2·K before dry-out occurred. An effective thermal conductivity of 5920 W/m·K was reported for the investigated T-OHP. Fourier transforms were employed for spectral analysis of the pressure signal, and it was found that the signal did not exhibit oscillations at distinguishable characteristic frequencies; however, details of the spectral analysis pertinent to noise filtering, averaging, conditioning, etc., were not provided.

Most T-OHP characterization experiments neglect T-OHP wall/-container conduction effects when relying on external surface temperature measurements and incorporate either transparent media or employ neutron radiography for observing fluid oscillations. The current study experimentally investigates the oscillating fluid temperature within an operating, pure-copper T-OHP and relates it to external container temperature measurements. The internal/external temperatures are compared to determine the effects of T-OHP material conduction. Based on internal fluid temperature measurement, the heat transfer coefficient in the adiabatic region is estimated. The actuality of fluid temperature oscillations is elucidated by characterizing their frequency, amplitude and mean temperature. Unlike Mameli et al. [36], the spectra of internal and external temperature signals are analyzed directly, instead of relying on a fluid pressure signal. An averaging/subtraction technique is also used to reduce spectral variance attributed to noise in order to calculate more representative characteristic frequencies. Because pairs of internal/external temperature signals were recorded in the adiabatic region, spectral subtraction is used to mitigate noise effects associated with reducing the spectral contribution from circulation/changes in bulk fluid arrangement that occur at a longer time scale. It will be shown that the actual temperature oscillations within the adiabatic section of the T-OHP are more drastic, frequent, and have a higher mean temperature than external temperature measurements suggest.

2. Experimental Setup and procedure

A 4-turn tubular OHP, as shown in Fig. 2, was fabricated from 3.25 mm ID, 4.8 mm OD deoxidized high phosphorus copper (C12200 alloy) tubing. The upper limit on an OHP's channel size for inducing capillary action depends on the employed working fluid and local gravitational conditions. The critical internal radius of OHP channels for non-microgravity conditions is well-established and shown in Eq. (1) [37], *i.e.*:

$$\mathrm{Bo} = \frac{r^2 g(\rho_{\mathrm{liq}} - \rho_{\mathrm{vap}})}{4\sigma} < \mathrm{Bo}_c \tag{1}$$

where Bo_c is the critical Bond number for capillarity (~4 for 1 g conditions). As seen in Fig. 2, ten type-T TCs were affixed to the outside wall of the T-OHP using a high temperature adhesive (Loctite® 495). Two were located in the evaporator, six in the adiabatic region, and two in the condenser. In addition, three type-T TCs were placed inside the T-OHP for direct temperature measurement of the working fluid. The TC beads (*i.e.* where the two wires have been welded together to form the measurement junction) were spherical in shape and approximately 0.8 mm in diameter. The 'internal' TCs were inserted into the T-OHP through three circular holes located

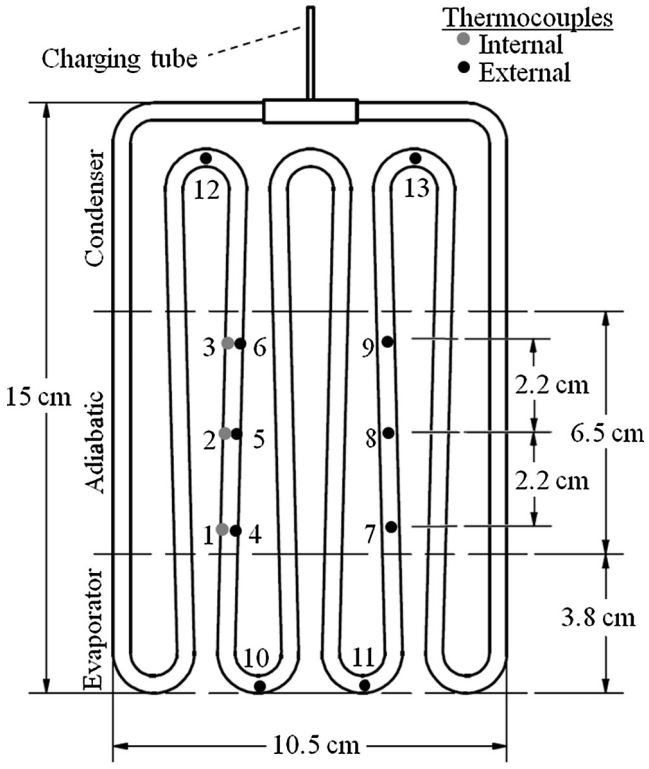

Fig. 2. Dimensions of investigated T-OHP with approximate evaporator, condenser and TC locations.

along the adiabatic region, and the TC beads were positioned as to be at or near the center of the T-OHP tube. The axial locations of the internal TCs matched those of the external adiabatic TCs with ±0.5 mm certainty. A short, tubular (1.6 mm OD, 0.9 mm ID) copper section was joined to each circular hole using tin-lead solder to support the internal TC wires. A sectional view of one of these 'ports', as well as the dimensions and relative internal/external thermocouple locations, is shown in Fig. 3. It is worth noting that each internal TC obstructed ~18% of the flow area (including both the TC bead and wire). This flow obstruction surely affected the fluid flow to some degree, and thus heat transfer, in the measured tube section. However, the current study focuses more on documenting the variation in recorded temperature between fluid-side/internal and wall-side/external thermocouples, for ultimately characterizing capacitive effects of the interposing tube wall and in estimating local heat transfer coefficients. The degree to which the inserted thermocouples affect T-OHP thermal performance was not measured.

Each copper port housing was crimped around the TC wire and filled with epoxy (Loctite® 495) to secure the wires and to act as a sealant. A section of plastic tubing (1.6 mm ID, 3.2 mm OD) was then placed over the port/wires and filled with silicone-based vacuum grease (Dow Corning® High-Vacuum Grease) to form a redundant seal. After the three internal TCs were in place, the T-OHP was attached to a centrifugal vacuum pump (Fisher Scientific® M8C) in line with a cold trap assembly for its evacuation to less than ~1 Pa. To test the hermeticity of the TC ports, the T-OHP was temporarily sealed for several hours. During this time, the T-OHP was confirmed to maintain its initial vacuum pressure via a pressure meter connected in line with the T-OHP. Via the vacuum pump, the T-OHP was again evacuated to ~1 Pa before being charged with HPLC-grade water (Fisher Chemical® W5SK-4) to a 75% (±2%) filling ratio. The open end of the T-OHP charging tube (see Fig. 1) was then pneumatically crimped and momentarily immersed in molten lead solder.

As shown in Fig. 4, one side of the top ~30% of the T-OHP length was firmly clamped to an aluminum water/cooling block to create the condenser boundary conditions. The opposite side of the T-OHP was insulated with aerogel insulation to promote heat transfer to only the cooling blocks. Refrigerated water was continuously routed through the water blocks' four channels (which were connected in series) at ~20 °C by a circulating bath (PolyScience AD15R-30-A11B). Below the adiabatic section, and on the same side of the T-OHP as the water blocks, an aluminum heating block was firmly attached for simulating the evaporator boundary condition, providing a heated length ~30% of the T-OHP length. The heating block held five 150 W cartridge heaters (Watlow FIREROD), approximately 6.35 mm in diameter and 3.2 cm in length. Thermal paste (Omegatherm 201) was applied to the surfaces of the T-OHP in contact with the heating block and water block to reduce thermal contact resistance between the circular OHP tube and the flat heat/cooling blocks. Thermal paste was also applied around all cartridge heaters. The entire T-OHP assembly was wrapped in fiberglass insulation to minimize heat loss to environment. Nonetheless, heat loss from the T-OHP assembly existed and was found to increase with power input, predominantly near the evaporator. Heat loss from the T-OHP surface during experimentation was measured to be approximately 10% at higher power inputs (i.e. >200 W).

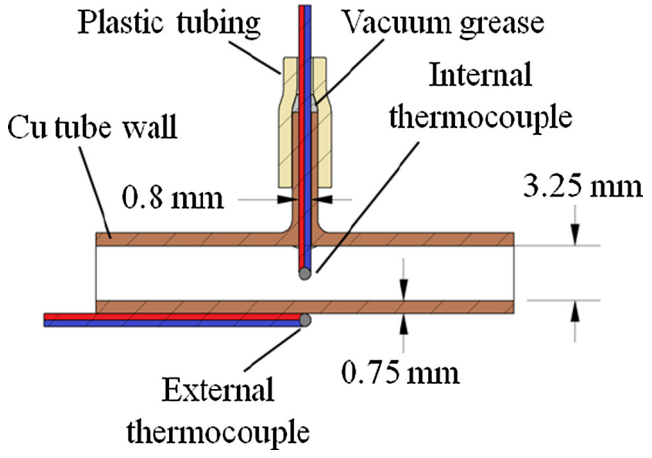

Fig. 3. Copper OHP tube wall (with dimensions) and perpendicular, copper thermocouple insertion port (with 0.8 mm inner diameter) wrapped with plastic tubing and vacuum grease. Typical positioning of external and internal thermocouples is also shown.

Power supply to cartridge heaters was controlled by a variable autotransformer monitored with a digital multimeter (DMM). Testing of the T-OHP began with a power input near ~60–75 W. Power was then increased in increments of 25 W until internal temperature exceeded 100 °C. Upon introduction of a new power input, the T-OHP temperature field was allowed to achieve a pseudo steady-state, and then approximately three minutes of steady-state temperature measurements were recorded. It is worth noting that the temperature field of the T-OHP began oscillating at power inputs less than 60 W (as low as 40 W), but these thermal oscillations were not sufficiently steady until ~60 W. Thermal data were collected by a data acquisition (DAQ) system (National Instruments® cDAQ-9178 chassis with a NI-9213 temperature module) and processed using LabVIEW. All TCs were sampled at a rate of 300 Hz and temperature variation was measured with a resolution of 0.25 °C. All tests were performed in the vertical, bottom-heating mode shown in Fig. 4.

3. Results and discussion

3.1. Temperature signal analysis

Internal and external temperature signals were analyzed in both the time and frequency domains. For signals in the frequency domain, the short-time Fourier transform was used to estimate the amplitude spectra. Prior to computing amplitude spectra, each temperature signal was shifted to oscillate about zero by subtracting its temporal mean from each raw value (over the sampling period). The discrete Fourier transform of the zero-shifted temperature signal, x[n], is then defined as [38]:

$$X[m] = \sum_{n=0}^{N-1} x[n] \exp(-2\pi j m n / N) \tag{2}$$

where $0 \le n < N$, N is the number of samples recorded, Δt is the sampling period (if the signal is sampled at frequency f_s, then $\Delta t = 1/f_s$) and $n\Delta t$ is time (in seconds) from initiation of each data string. The amplitude spectrum of x[n] is then:

$$S[m] = \begin{cases} \frac{1}{N}|X[m]|, & m = 0 \text{ or } m = \lfloor \frac{N+1}{2} \rfloor \\ \frac{2}{N}|X[m]|, & 0 < m < \lfloor \frac{N+1}{2} \rfloor \end{cases} \tag{3}$$

where $0 \le m \le \lfloor N/2 \rfloor$. The amplitude spectrum in Eq. (3) gives the peak magnitude of the Fourier component at frequency $m/(N\Delta t)$. When considering the amplitude spectrum of a signal, a common practice is to split the full signal into several segments of equal duration, then to average the amplitude spectra of each of these segments [39]. This process reduces the variance of the spectrum estimate, at the cost of frequency resolution. This approach was used herein, and each signal was split into segments of $n = 2048$ (2^{11}) samples prior to computing the average amplitude spectrum; providing for a frequency resolution of 0.148 Hz.

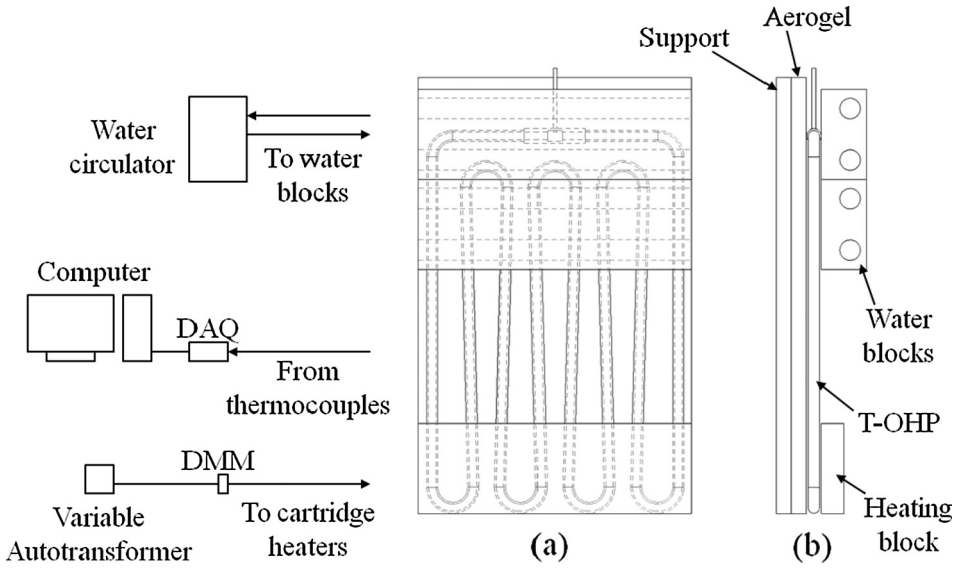

Fig. 4. Experimental schematic and (a) front and (b) profile view of T-OHP test assembly (fiberglass insulation not shown).

The internal/external temperature signals and amplitude spectra, corresponding to each internal TC location (as shown in Fig. 2) during OHP operation at a power input of 275 W, are shown in Figs. 5–7. The spectra in Figs. 5–7 are typical and representative of all investigated power inputs investigated as data were recorded only for power inputs that resulted in steady fluid oscillations. The only major difference in the amplitude spectra for various power inputs was the location of the local peak amplitude maxima, which corresponded to lower frequencies at lower power inputs. As shown in Figs. 5(b), 6(b), and 7(b), the local maximum was at ~4 Hz for a power input of 275 W; however, the maximum was ~3 Hz or ~2 Hz for power inputs of 150 W and 60 W, respectively. The oscillation peak amplitudes also varied along the T-OHP length most likely due to the non-uniform, axial-wise liquid/vapor distribution and fluid motion inside the OHP. The liquid and vapor slug motion is analogous to a multiple mass-spring-damper system being excited at one end (*i.e.* the evaporator) [40], which causes higher frequency oscillations to dampen along the length of the tube. The current OHP consisted of a relatively high filling ratio, resulting in it possessing an evaporator and condenser predominantly filled with vapor and liquid, respectively, during its steady-state operation.

It is clear from Figs. 5(b), 6(b), and 7(b), that the OHP temperature oscillations consist of multiple frequencies and that the internal, fluid-submerged TCs capture temperature fluctuations with higher amplitudes and frequencies relative to those collected by the external TCs attached to the tube wall. This behavior is evident in both time and frequency domains; becoming more apparent at locations closer to the evaporator. In general, the external TC temperature oscillations possessed frequencies an order-of-magnitude less than those of the internal TCs, *i.e.* ~1 Hz vs. ~10 Hz, respectively. The higher-frequency temperature fluctuations are attributable to the local, oscillatory slug motion in the adiabatic region of the T-OHP, while the lower-frequency (≤0.5 Hz) components, shared between both signals, exist due to the longer time scale fluid behavior within the T-OHP such as: bulk fluid rearrangement (*i.e.* cross-channel circulation) and/or occasional pauses/reduction in fluid motion [24]. This behavior is documented in other studies that describe T-OHP oscillation modes [2–4,8].

The average temperature differences between individual pairings of internal and external TCs is defined in Eq. (4), *i.e.*:

$$\Delta T = \overline{T_i} - \overline{T_e} \tag{4}$$

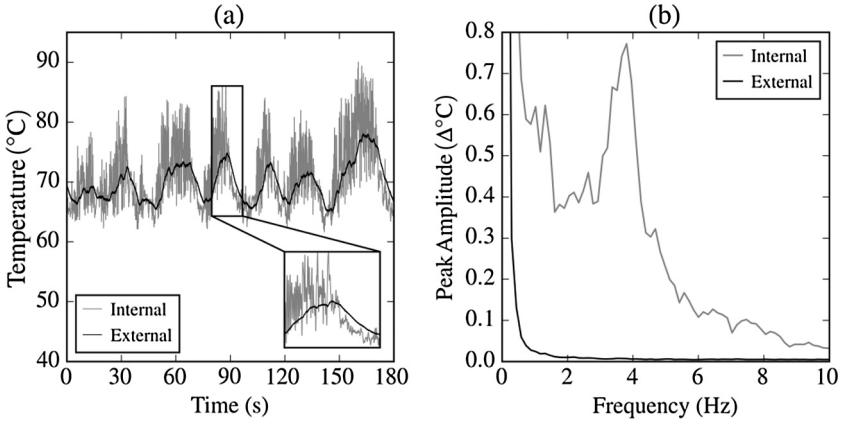

Fig. 5. (a) Internal and external steady-state temperature signals (with example cases of temperature lag indicated) and (b) amplitude spectra of internal and external temperature signals (T_1 and T_4) measured at the evaporator side of the adiabatic region with a 275 W power input.

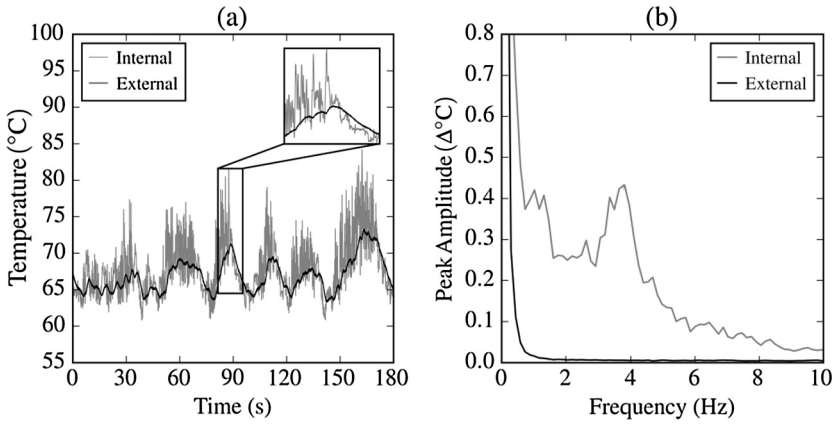

Fig. 6. (a) Internal and external steady-state temperature signals (with example cases of temperature lag indicated) and (b) amplitude spectra of internal and external temperature signals (T_2 and T_5) measured at the middle of the adiabatic region with a 275 W power input.

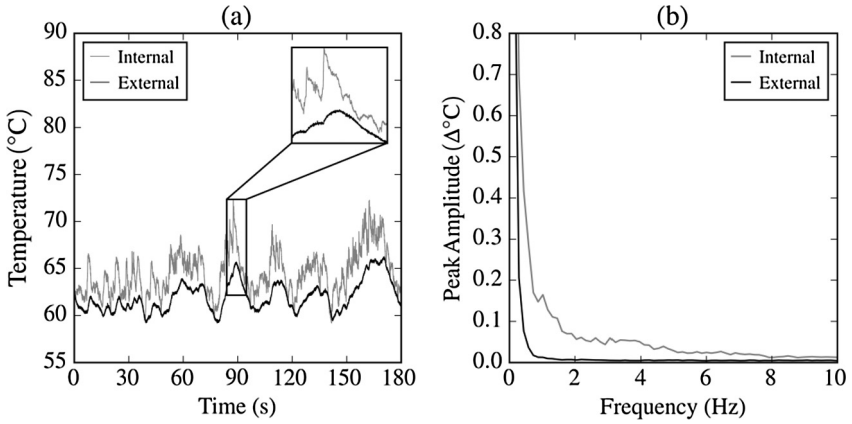

Fig. 7. (a) Internal and external steady-state temperature signals (with example cases of temperature lag indicated) and (b) amplitude spectra of internal and external temperature signals (T_3 and T_6) measured at the condenser side of the adiabatic region with a 275 W power input.

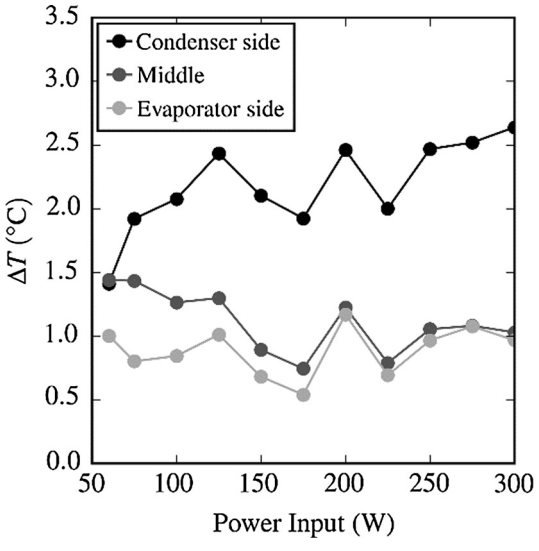

Fig. 8. Difference between average internal and external temperature for the evaporator-side, middle, and condenser-side TC pairs.

These average temperature differences are shown in Fig. 8, where it may be seen that the temperature difference of the condenser-side TC pair is approximately double that of the middle/adiabatic and evaporator-side TC pairs. This exposes an axial-wise, constant temperature gradient along the OHP tubular structure that is near-independent of the internal fluid motion and heat transfer due to the imposed heating/cooling conditions but that are significantly less in magnitude relative to the longitudinal gradient. As a result, the heat transfer between the internal working fluid and tubular wall is dependent on axial position between the evaporator and condenser.

These results motivate the discussion of an OHP 'thermal impedance'. Such thermal impedance, analogous to electrical impedance, is primarily a function of the tube wall conduction resistance and its thermal capacitance. The thermal 'impedance', *i.e.* the time-variant thermal resistance, of the tube wall and contact interface, 'dampen' and phase-shift the oscillatory heat transfer as it conducts into and then along the tube wall from the agitated, pulsating fluid within the OHP. This increased thermal impedance results in the externally-measured temperature oscillations possessing smaller amplitudes and phase-shifts relative to those measured by internal TCs. The temperature signals provided in Figs. 5–7(a) reveal a time lag between the internal and external TC measurements. Temperature peaks (and valleys) measured by the internal TCs are not immediately experienced by the external TCs, with internal and external temperature signals closest to the evaporator being most unsynchronized. This time lag exists due to the finite time required for a change of internal temperature to transmit through the tube wall and across the tube wall/external TC interface, and then be registered by the external TC and DAQ

system. In order to quantify this behavior, the average time lag, τ, between changes in the measured internal and external temperatures, is estimated by maximizing the normalized cross correlation of the internal and external temperature signals. The normalized cross correlation at a delay of d samples is given by [39]:

$$R_{xy}[d] = \frac{\frac{1}{N}\sum_n x[n]y[n+d]}{\sqrt{\frac{1}{N}\sum_n (x[n])^2}\sqrt{\frac{1}{N}\sum_n (y[n])^2}} \quad (5)$$

where x[n] and y[n] ($0 \le n < N$) denote the measured internal and external temperatures, shifted to oscillate about zero by subtracting their respective mean values. The normalized cross correlation function gives a measure of similarity between the internal temperature signal and a time-shifted version of the external temperature signal (shifted backward in time by d samples, *i.e.* $d\Delta t$ seconds). Hence, the average τ between the internal and external temperature signals may be estimated by finding the delay d which maximizes $R_{xy}[d]$:

$$\tau = \Delta t \cdot \mathrm{argmax} R_{xy}[d]. \quad (6)$$

Histograms of the average time lags calculated using Eq. (6) are shown in Fig. 9; a uniform bin width of 0.25 s was employed. As shown in Fig. 9, the time lags range from ~1 s to ~2 s. The average τ increases for locations closer to the evaporator and for increasing OHP power inputs. The relation between τ and location is likely due to the varying temperature difference between the oscillating fluid and the wall (shown in Fig. 8). Because there is a larger radial temperature gradient near the condenser, there is a faster transient 'jump' in external temperature. This temperature jump is more readily observed by the condenser-side external TC than the evaporator-side TC (where a smaller mean temperature difference exists). Additionally, due to the filling ratio of the T-OHP (75%), very few vapor plugs would have passed the condenser-side internal thermocouple (T_3) relative to the middle and evaporator-side locations (T_2 and T_1, respectively). Thus, the local convection coefficient would have varied longitudinally due to the differing prevalence of liquid/vapor at the three locations.

Because the working fluid exhibits multi-modal oscillatory behavior (*i.e.* bulk fluid rearrangement, etc. vs. local fluid motion), spectral subtraction was used in an attempt to separate the long time scale phenomena captured by both internal and external TCs from the actual slug oscillations captured by the internal TCs. This was achieved by subtracting the external amplitude spectrum from the internal amplitude spectrum. Fig. 10 provides the internal/external temperature amplitude spectra, and their difference, for the T_2 & T_5 location (*i.e.* middle adiabatic) for the OHP operating at power inputs of 60 W, 125 W, 225 W, and 300 W. It can be seen in Fig. 10 that the internal frequencies and external amplitudes tend to increase with OHP power input. Despite the spectral subtraction, the internal spectrum retains components at lower frequencies due to the higher amplitudes seen in Figs. 5–7.

A mean, local frequency was defined for each signal x[n] to facilitate direct comparison of the amplitude spectra, *i.e.*:

$$f_{mean} = \frac{\sum_{n=0}^{\lfloor N/2 \rfloor} f_n S[n]^2}{\sum_{n=0}^{\lfloor N/2 \rfloor} S[n]^2}. \quad (7)$$

where $f_n = n/N\Delta t$. While the mean frequency has utility in representing a signal's amplitude spectrum with a single number, the signal may or may not contain any oscillations at the mean frequency. The mean frequencies given by Eq. (7) for each temperature signal are *local* in that they characterize temperature fluctuations at particular locations along the length of the tube (as seen in Figs. 5–7). However, a spatially-averaged frequency is also desired in order to compare results with models that predict only single characteristic oscillation frequencies. If the mean frequency at location x_i is denoted as $f_{mean,i}$, such a characteristic frequency *barf* may be calculated by spatially averaging the local mean frequencies. Numerical integration may be used to average the local mean frequencies over space; here, since the mean frequencies were calculated at an odd number of locations ($N = 3$), the trapezoidal rule was used to find the spatially-averaged mean frequency.

$$\bar{f} = \frac{\frac{1}{2}\sum_{i=1}^{N-1}(f_{mean,i+1} + f_{mean,i})(x_{i+1} - x_i)}{x_N - x_1} \quad (8)$$

The difference between the internal and external amplitude spectra may be used with Eq. (7) to estimate the local slug oscillation frequency at each TC location. These local frequencies may then be used in Eq. (8) to estimate a mean (spatially-averaged) slug oscillation frequency. These local, mean oscillation frequencies are shown for each OHP power input in Fig. 11(a). Analytically-predicted oscillation frequencies from Furukawa [33] are also provided in Fig. 11(b) for comparison with the overall (spatial) mean frequency. Fig. 11 shows that the local oscillation frequency at the middle and evaporator side increases with increasing power input (from ~1.5 Hz at 60 W to ~2.5 Hz at 300 W), and this is consistent with Figs. 5–7. The spatially-averaged mean temperature oscillation frequency also increases with increasing power input, suggesting that the frequency of fluid oscillations increases as the power input increases. Although Furukawa's model underestimates the observed slug oscillation frequency by ~30%, it predicts a similar increase in oscillation frequency with power input. Note

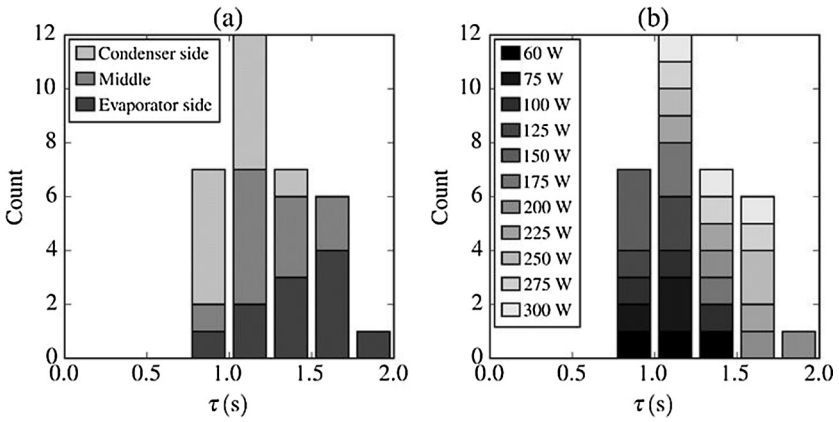

Fig. 9. Histograms of time lags, (a) grouped by location (includes all power inputs) and (b) grouped by power input (includes all locations).

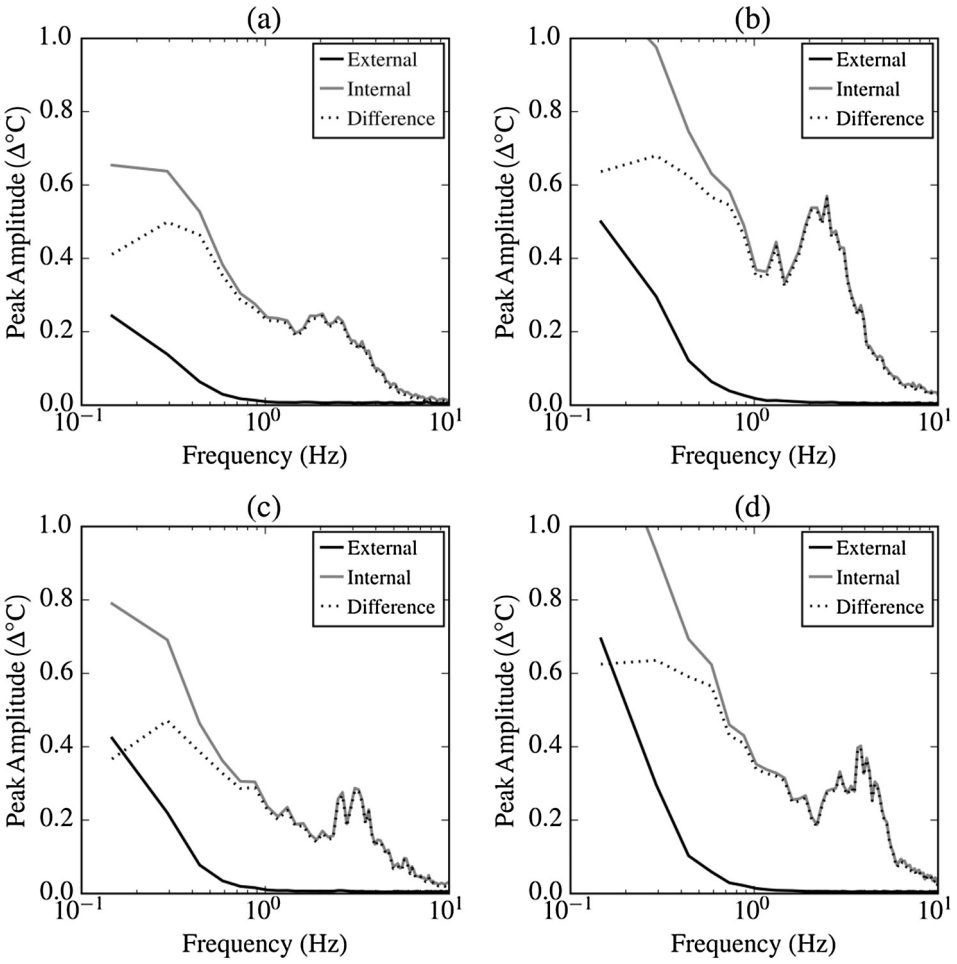

Fig. 10. Internal and external amplitude spectra of temperatures measured at the T_2/T_5 location, and their difference, for power inputs of (a) 60 W, (b) 125 W, (c) 225 W, and (d) 300 W.

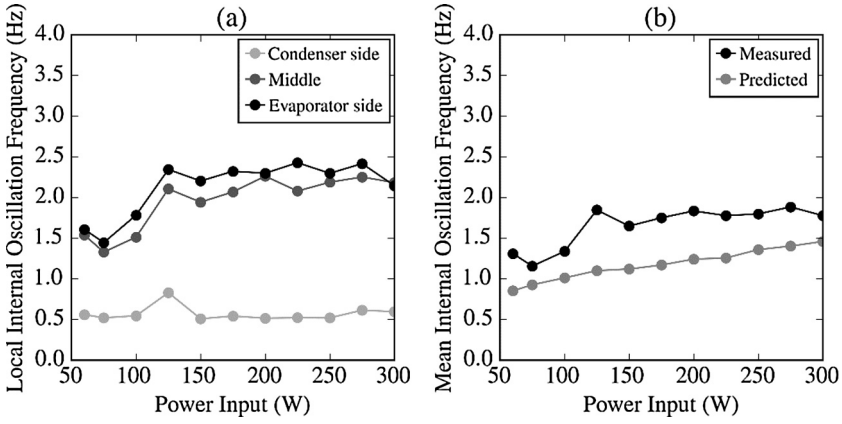

Fig. 11. (a) Local oscillation frequency vs. power input at each measurement location; (b) measured and predicted mean oscillation frequency vs. power input.

that the reported oscillation frequencies correspond to temperature measurements, not directly with fluid pulsation, although it is reasonable to consider them to be approximately equivalent.

As shown in Figs. 5–7, when internal temperatures change slow enough (*i.e.* during intermittent periods of reduced fluid oscillations), the external temperature follows closely in magnitude. However, in the presence of high frequency oscillations, the transient conduction through 0.5 mm of copper and across the external TC/wall interface creates a noticeable temperature difference. This suggests that the thermal network between the internal and external TCs acts as a filter, since temperature oscillations at certain frequencies in the 'input' signal (internal temperature) are not present in the 'output' signal (external wall surface temperature). If the thermal network between the TCs is idealized as a single-input, single-output filter, then the frequency response function of the 'filter' quantifies the degree to which it attenuates temperature oscillations, as a function of oscillation frequency. The temperature frequency response function may be approximated as [39]:

$$H[m] = \frac{|X^*[m]Y[m]|}{|X[m]|^2} \tag{9}$$

where H[m] is the gain ratio at frequency $m/(N\Delta t)$, x[n] and y[n] denotes the internal and external temperature signals, X[m] and Y[m] denote the discrete Fourier transforms of x[n] and y[n], X*[m] denotes the complex conjugate of X[m]. The gain of the filter, in decibels, is given by:

$$\text{Gain}[m] = 20 \log \text{H}[m]. \tag{10}$$

Note that the same averaging technique that was used to compute the amplitude spectra was also used to compute the frequency response functions. Applying this analogy to filters, Fig. 12 shows the filter gain at the middle location for power inputs of 60 W, 125 W, 225 W, and 300 W. Since most of the thermal network between the internal and external TCs remained unchanged as the power input was varied in this study (convection resistance would vary based on fluid behavior), the frequency response function was expected to take on a similar shape for all power inputs; Fig. 12 agrees with this expectation. Additionally, the authors note that the frequency response function depends not just on the fluid and material properties and OHP geometry, but also on details of the measurement system such as the type of TCs used and the method of TC attachment.

From Fig. 12, it may be seen that the gain decreases rapidly between 0 Hz and 2 Hz, and this observation agrees with Figs. 5(b), 6(b), and 7(b), and 8, where oscillations at frequencies ≥2 Hz appear in the amplitude spectra of the internal temperature signals but not in the amplitude spectra of the external temperature signals. Furthermore, these results are consistent with what was predicted by Xue et al. [25]. Although the density and specific heat ratios between the TC bead and T-OHP tube are near unity, the thermal conductivity of the copper-constantan bead (assumed to be 77% Cu and 23% Ni) is ~50 W/m·K [41]—approximately 13% that of the copper tube. Xue et al. estimated that a 'k-ratio' of this magnitude (with all other parameter ratios at unity) would result in ≥95% attenuation of frequencies larger than 1 Hz, and this is neglecting the impact of contact resistance. Thus, it is unrealistic to assume that the external temperature measurement arrangement described in the current study (type-T TCs mounted on copper) would capture the true oscillation behavior of an OHP fluid, especially when considering the interfacial resistance between the TC bead and wall. For the internal temperature measurements, the TC-to-liquid k-ratios are favorable ($\alpha_{TC}/\alpha_{liq} \approx 90$), but the very low relative density of the water vapor is not conducive for transient measurements ($\alpha_{TC}/\alpha_{vap} \approx 10^{-2}$). Therefore, the fact that liquid slugs are intermingled with the vapor plugs is important for obtaining reliable internal frequency measurements, especially near the evaporator where vapor is more prevalent. However, because of the relatively high filling ratio used in this study (75%), neither evaporator dry-out or high vapor quality occurred for the range of power inputs investigated.

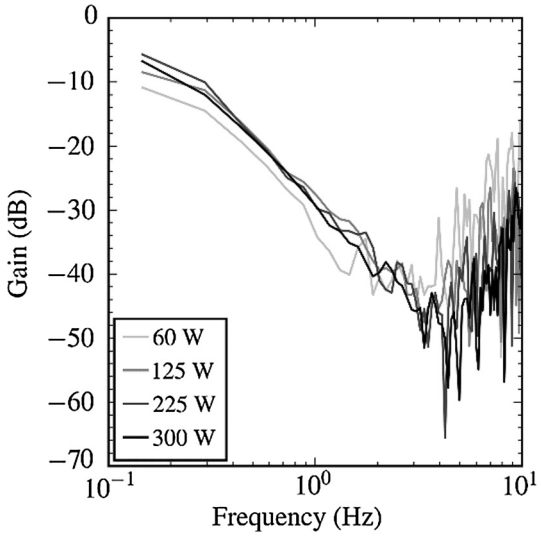

Fig. 12. Frequency transfer function for power inputs of 60 W, 125 W, 225 W, and 300 W computed using temperatures measured at the middle of the adiabatic region.

It should be noted that the temperature oscillation analysis presented herein may not be directly application to FP-OHPs. Smoot et al. [42] demonstrated that FP-OHP inter-channel conduction reduces the amplitude of external temperature oscillations. Although the OHP with interconnected channels may give better high heat flux performance than a traditional T-OHP design, the added effect of inter-channel conduction likely alters the results and interpretations presented herein. Also, because there are many geometric/operating parameters that influence fluid oscillation frequency, even similar-shaped T-OHPs may yield different results than those presented here.

3.2. Thermal performance

OHP thermal performance is commonly quantified via an evaporator-to-condenser thermal resistance or effective thermal conductivity, with both measures accounting for the multiple heat transfer modes existent within an OHP. The T-OHP's effective thermal resistance for each operating power may be estimated using:

$$\psi_{\text{eff}} \approx \frac{\Delta T_{\text{OHP}}}{P} \tag{11}$$

where ΔT_{OHP} is the external, average temperature difference across the T-OHP. With reference to TC locations shown in Fig. 2, ΔT_{OHP} is defined as:

$$\Delta T_{\text{OHP}} = \text{avg}(T_4, T_7, T_{10}, T_{11}) - \text{avg}(T_6, T_9, T_{12}, T_{13}) \tag{12}$$

where the spatial and temporal average of each TC group are taken. The effective thermal conductivity of the T-OHP may be estimated as:

$$k_{\text{eff}} \approx \frac{P}{8(\pi/4d_o^2)} \left(\frac{\Delta z}{\Delta T}\right)_{\text{adia,avg}} \tag{13}$$

where $(\Delta T/\Delta z)_{\text{adia,avg}}$ is the average temperature gradient across the adiabatic region calculated using the temperatures at the three longitudinal measurement locations shown in Fig. 2. The temperature gradient was calculated in two ways for each power input, (1) using only the internal temperature signals (*i.e.* $T_{1\text{-}3}$) giving $k_{\text{eff,i}}$ and (2) using only the external temperature signals (*i.e.* $T_{4\text{-}9}$) giving $k_{\text{eff,e}}$. The effective thermal resistance is plotted against T-OHP power input in Fig. 13(a), while these two thermal conductivities are plotted against T-OHP power input in Fig. 13(b). The relative percent difference between the internal and external thermal conductivities, calculated using Eq. (14), is shown in Fig. 13(c).

$$\Delta\% = \left|\frac{k_{\text{eff,i}} - k_{\text{eff,e}}}{k_{\text{eff,e}}}\right| \cdot 100 \tag{14}$$

As shown in Fig. 13, the T-OHP achieved $k_{\text{eff}} \sim 15{,}000$ W/m·K ($\psi_{\text{eff}} \sim 0.05$ K/W) at the highest power input investigated, which is ~38 times higher than that of pure copper. Eq. (13) assumes no heat loss, however, even if a relatively high 20% heat loss is considered, the maximum k_{eff} would still be ~12,000 W/m·K ($\psi_{\text{eff}} \sim 0.06$ K/W). Both Fig. 13(a) and (b) demonstrate trends indicating that the T-OHP's thermal performance increases with increasing power input, which is typical. Due to the conduction

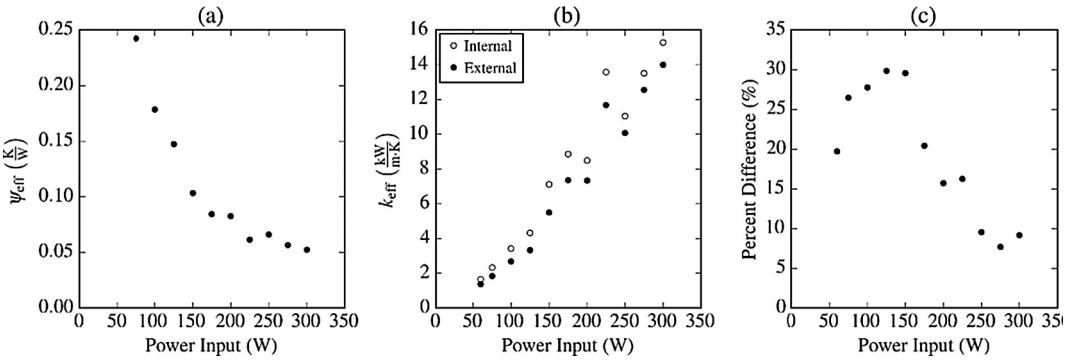

Fig. 13. T-OHP thermal performance quantified using (a) thermal resistance and (b) effective thermal conductivities calculated using either internal or external adiabatic thermocouples. The relative percent difference in k_{eff} calculations using internal or external temperature is shown in (c).

resistance of the tube wall, and rapid internal fluid advection, the radial-wise temperature gradient varies along the axial direction. For these reasons, $k_{eff,i}$ is distinctly larger than $k_{eff,e}$ as shown in Fig. 13(b). This difference between $k_{eff,i}$ and $k_{eff,e}$ is a function of power input, as seen in Fig. 13(c), and this can be explained by how an OHP's fluid distribution varies with power input. For an axial, bottom heated OHP, the evaporator region is, more often than not, initially flooded with liquid at low heat inputs due to gravity [43], although capillary forces can allow vapor plugs to form throughout a OHP at room temperature. Once fluid oscillation begins, the liquid is pressed into the adiabatic region and condenser as vapor forms and expands in the evaporator. Until evaporator dry-out, liquid can still be forced into the furthest extents of the evaporator (geometrically defined in Fig. 2 by the outline of the heating block). However, during normal OHP operation vapor and liquid are the most common phase in the evaporator and condenser, respectively. At steady-state there exists boundaries for the predominately vapor/liquid regions that form in the evaporator and adiabatic/condenser sections, respectively. The filling ratio for the currently-investigated T-OHP was ~75%, meaning the average vapor/liquid boundary would have been at or near the edge of the evaporator for low power inputs. However, at higher power inputs, this boundary would have progressed into the lower adiabatic region as the amplitude of fluid motion increased due to higher vapor pressures, and this could have changed the prevailing measurement conditions for the internal TCs (especially for T_1).

Most predictive OHP performance models are either numerical or analytical in nature, often employing experimental data for validation [14,40]. In most cases, these models do not incorporate surface/fluidic temperature data during their development. Although some models focus on the interaction of the liquid and vapor slugs and their subsequent impact on performance, the effect of OHP material and wall thickness (and subsequent conduction) is often neglected. For those empirical OHP models/correlations [44–48] that require experimental data as input, Fig. 13 shows that such models are sensitive to the measurement location, or source, of such data, *i.e.* if temperatures were measured (or estimated) inside the OHP or along the OHP surface only. This difference is largest at low heat inputs when fluid oscillations are lowest.

3.3. Internal heat transfer coefficient

From Fig. 8 it may be seen that the temperature difference between the fluid and the internal wall of the T-OHP is not constant along the length of the adiabatic region, with the axial temperature gradient along the OHP wall being typically larger than that of the fluid. As mentioned, this is due to the hot fluid motion from the evaporator to the condenser, which occurs at a shorter time scale than longitudinal conduction along the tube wall. This temperature potential results in convection between the fluid and the tube wall, resulting in a change in fluid enthalpy. Assuming the temperature gradient in the radial direction is relatively small, external temperature measurements were used to quantify longitudinal conduction heat transfer along the length of the adiabatic section. The assumption that the exterior tube wall section between the evaporator and condenser is adiabatic (as shown in Fig. 14) is likely valid due to the large ratio of radial to longitudinal thermal resistance. Fig. 14 provides a schematic for the employed internal heat transfer model. The longitudinal conduction heat transfer rate along the tube wall (between T_4 & T_5 and T_5 & T_6, respectively) was estimated using Fourier's law, i.e.:

$$q_{cond} = -k_{Cu} A_{c,w} \frac{\Delta T}{\Delta z} \tag{15}$$

Fig. 15 shows the calculated conduction heat transfer rate in a single tube for all OHP power inputs. It may be seen that longitudinal conduction along the tube wall plays only a minor role in overall T-OHP heat transfer. At the minimum power input investigated (60 W), the total wall conduction provided for ~10% (~0.75 W × 8 tubes = ~6 W) of the total heat transfer. The conduction heat transfer decreased to less than 2% of the overall T-OHP heat transfer as the power input increased and fluid advection

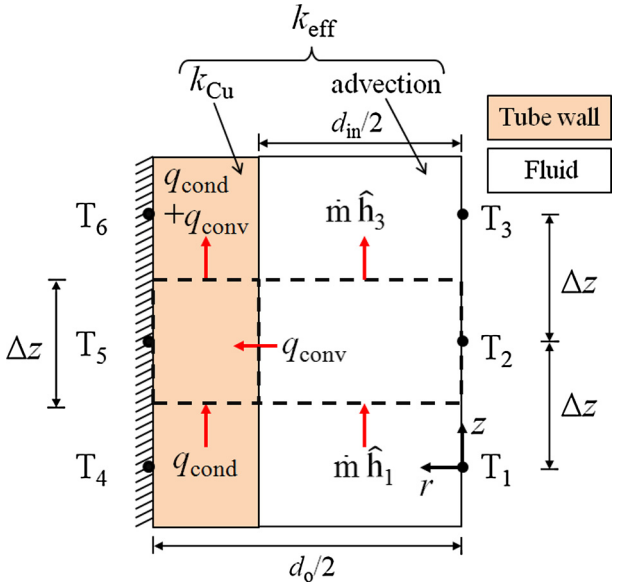

Fig. 14. Internal OHP heat transfer model used to estimate the local, single phase heat transfer coefficient in the OHP adiabatic.

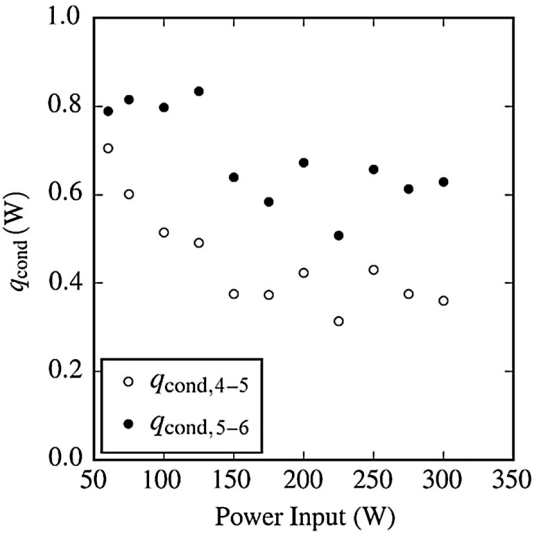

Fig. 15. Longitudinal conduction heat transfer rate in a single OHP tube wall vs. power input in the lower and upper adiabatic region.

strengthened. It is observed that $q_{cond,5\text{-}6}$ is larger than $q_{cond,4\text{-}5}$, meaning energy was added to the copper wall from the fluid via convection. Based on the heat added to the wall by convection (*i.e.* the difference between $q_{cond,4\text{-}5}$ and $q_{cond,5\text{-}6}$), the interior heat transfer coefficient was estimated as:

$$h_{sp} \simeq \frac{q_{conv}}{A_{c,w}(T_2 - T_5)} \simeq \frac{q_{cond,5-6} - q_{cond,4-5}}{A_{c,w}(T_2 - T_5)} \tag{16}$$

Because the T-OHP was filled with water at a 75% filling ratio, it is assumed that the majority of the adiabatic region consistently experienced oscillating liquid during operation. However, this assumption becomes less valid at higher heat inputs when amplitude of fluid motion increases. The single phase Nusselt number was also calculated using Eq. (17)

$$Nu_{D,sp} = \frac{h_{sp} d_{in}}{k_{H_2O}} \tag{17}$$

where k_{H2O} is the thermal conductivity of liquid water at the average of T_2. Fig. 16 shows the local, single phase heat transfer coefficient and Nusselt number, which is proportional to h_{sp} by a factor of d_{in}/k_{H2O}. It can be seen that h increases from the minimum power input until ~150 W, where a maximum of ~1130 W/m^2·K is reached. From 150 to 300 W, h fluctuates about a mean of ~910 W/m^2·K. Since the convection coefficient of turbulent flow in a tube is a function of the Reynolds and Prandtl numbers, these values of h would differ if the working fluid were changed or if the channel geometry were altered. The single-phase Nusselt number along the adiabatic section varied between 4 and 6.

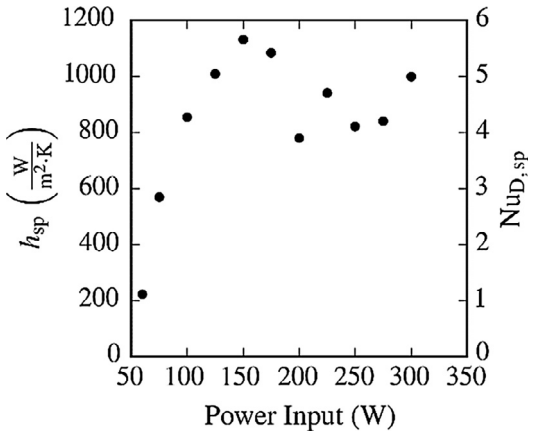

Fig. 16. Internal, local heat transfer coefficient and Nusselt number for single phase convection vs. power input in center (axially) of adiabatic region.

The drop in h after 150 W matches the drop in difference between $k_{eff,i}$ and $k_{eff,e}$ in Fig. 13(c). The majority of OHP heat transfer is sensible [14,15], therefore both h and Nu were calculated using the assumption of (predominately) single phase flow in the adiabatic region. As a result, the increased vapor presence in this region at higher power inputs could drastically affect the accuracy of Eqs. (16) and (17) at higher power inputs. Combining this experiment with a fluid visualization method (*e.g.* neutron radiography) would provide insight into when the single-phase convection coefficient assumption breaks down.

4. Conclusions

Using pairs of thermocouples (TCs) placed inside and atop an operating T-OHP, it was observed that the external, surface temperature measurements of the T-OHP did not replicate temperature measurements within the T-OHP due to the thermal impedance of the tube wall and external TC attachment method. Only large time-scale behavior (typically < 1 Hz) accompanying bulk fluid motion was captured by the external TCs. Measuring the temperature of the internal, pulsating working fluid during OHP operation also allowed the forced convection heat transfer between the OHP evaporator and condenser to be characterized. Since this sensible form of convection is a dominant mode of heat transfer within the OHP, knowledge of a heat transfer coefficient, and Nusselt number, should aid continual modeling efforts focused on OHPs. Major finding with additional comments are summarized below.

1. Internal temperature oscillations have a greater amplitude, frequency, and mean than those measured along the external walls of the adiabatic section of an OHP.
2. The internal TCs were able to capture oscillation frequency components up to ~5 Hz. The local, mean oscillation frequency for the evaporator side temperature ranged from 1.5 Hz to 2.5 Hz over the range of power inputs investigated (60–300 W), while the local oscillation frequency for the condenser side temperature remained fairly constant at about 0.5 Hz.
3. The frequency transfer function for the thermal network between the internal/external thermocouples was constant across all tested power inputs, which would be expected for a set tube wall and TC attachment method. The transfer function at 60 W was slightly different from 125, 225, and 300 W, but this is attributed to the lower internal convection coefficient observed from 60 to 100 W (with h being fairly constant from 125 to 300 W).
4. Large-scale temperature changes recorded by external TCs lagged behind corresponding internal measurements by a relatively constant amount (~1–2 s). The average time lag was found to increase slightly with decreasing distance from the evaporator and with increasing power input.
5. The conduction heat transfer rate along the OHP tube wall is not synced with heat transfer due to internal fluid advection. As a result, the temperature gradient along the wall is larger than the that along the fluid, and convection heat transfer between the fluid and wall thus occurs. This interaction lends one to question the validity of referring to the non-heated/cooled region of the OHP as 'adiabatic'.

6. The OHP effective thermal conductivity varies with axial distance along the OHP and depends highly on the temperature gradient used for its calculation. Since the effective thermal conductivity would be under reported when using only external temperature measurements, variation in k_{eff} would not be an issue for most applications if all design parameters and comparisons are consistently based on external temperature measurements.
7. The conduction along the tube wall accounts for only 2–10% of the overall heat transfer. Tube conduction is less significant at higher heat inputs when fluid advection increases.
8. The heat transfer coefficient associated with pulsating, single-phase fluid within the adiabatic region of the investigated OHP was estimated to be ~1000 W/m^2 K at power inputs larger than 100 W. The Nusselt number was found to vary between 4 and 6.

Knowing the relationship between external wall and fluidic temperature oscillations can be important when developing an OHP mathematical model or when characterizing the thermal performance of an OHP for a given application. However, the results presented here demonstrate the error in assuming external measurements accurately represent the internal fluid behavior. Due to wall conduction effects, an external temperature will have lower amplitude and frequencies than the internal temperature. This realization is important since, for instance, temperature oscillations with relatively high amplitude and frequency could negatively affect the mechanical integrity and performance of small or intricate OHPs due to thermally-induced stresses [49,50]. Understanding the thermal capacitance effects of the OHP container material during steady-state operation allows one to apply energy conservation models for determining conduction and convection heat transfer rates.

Acknowledgments

This work was sponsored in-part by the National Science Foundation under Awards # 1403872 & 1549973. Experimental work presented in this manuscript was obtained while J. Gabriel Monroe, Zachary Aspin, and John Fairley were students, and Dr. Scott Thompson an Assistant Professor, at Mississippi State University. Additional edits and contributions made by J. Gabriel Monroe, Zachary Aspin, and John Fairley during their employment by ERDC, CIS, and Sandia National Laboratories, respectively, were in a personal capacity. This work was not funded or endorsed by ERDC, CIS, or Sandia National Laboratories. Any opinions, findings, conclusions, or recommendations expressed herein do not necessarily reflect the views of ERDC, CIS, or Sandia National Laboratories.

References

[1] Akachi, H., 1990, Structure of a heat pipe, United States Patent: 4921041.
[2] G. Mahajan, H. Cho, S.M. Thompson, H. Rupp, K. Muse, Oscillating heat pipes for waste heat recovery in HVAC systems, in: ASME 2015 International Mechanical Engineering Congress and Exposition, ASME, 2015, p. V08BT10A003.
[3] J.G. Monroe, E.S. Vasquez, Z.S. Aspin, K.B. Walters, M.J. Berg, S.M. Thompson, Electromagnetic induction by ferrofluid in an oscillating heat pipe, Appl. Phys. Lett. 106 (26) (2015) 263901.
[4] S. Rittidech, N. Pipatpaiboon, P. Terdtoon, Heat-transfer characteristics of a closed-loop oscillating heat-pipe with check valves, Appl. Energy 84 (2007) 565–577.
[5] J. Gu, M. Kawaji, R. Futamata, Microgravity performance of micro pulsating heat pipes, Microgr. – Sci. Technol. 16 (2005) 181–185.
[6] N. Soponpongpipat, P. Sakulchangsatjaati, N. Kammuang-Lue, P. Terdtoon, Investigation of the startup condition of a closed-loop oscillating heat pipe, Heat Transfer Eng. 30 (November) (2009) 626–642.
[7] S. Wannapakhe, S. Rittidech, B. Bubphachot, O. Watanabe, Heat transfer rate of a closed-loop oscillating heat pipe with check valves using silver nanofluid as working fluid, J. Mech. Sci. Technol. 23 (2009) 1576–1582.
[8] B. Borgmeyer, H. Ma, Experimental investigation of oscillating motions in a flat plate pulsating heat pipe, J. Thermophys. Heat Transfer 21 (2) (2007) 405–409.
[9] S.M. Thompson, H.B. Ma, R.A. Winholtz, C. Wilson, Experimental investigation of miniature three-dimensional flat-plate oscillating heat pipe, J. Heat Transfer 131 (4) (2009) 43210.
[10] S.M. Thompson, P. Cheng, H.B. Ma, An experimental investigation of a three-dimensional flat-plate oscillating heat pipe with staggered microchannels, Int. J. Heat Mass Transfer 54 (2011) 3951–3959.
[11] S.M. Thompson, H.B. Ma, C. Wilson, Investigation of a flat-plate oscillating heat pipe with Tesla-type check valves, Exp. Therm. Fluid Sci. 35 (2011) 1265–1273.
[12] J.D. Fairley, S.M. Thompson, D. Anderson, Time–frequency analysis of flat-plate oscillating heat pipes, Int. J. Therm. Sci. 91 (2015) 113–124.
[13] N. Zhao, D. Zhao, H.B. Ma, Ultrasonic effect on the startup of an oscillating heat pipe, J. Heat Transfer 135 (7) (2013) 74503.
[14] M.B. Shafii, A. Faghri, Y. Zhang, Thermal modeling of unlooped and looped pulsating heat pipes, J. Heat Transfer 123 (December) (2001) 1159.
[15] M. Groll, S. Khandekar, Pulsating heat pipes: a challenge and still unsolved problem in heat pipe science, Arch. Thermodyn. 23 (4) (2002) 17–28.
[16] H. Ma, Oscillating Heat Pipes, Springer, 2015.
[17] H. Yang, S. Khandekar, M. Groll, Operational limit of closed loop pulsating heat pipes, Appl. Therm. Eng. 28 (2008) 49–59.
[18] M. Mameli, L. Araneo, S. Filippeschi, L. Marelli, R. Testa, M. Marengo, Thermal response of a closed loop pulsating heat pipe under a varying gravity force, Int. J. Therm. Sci. 80 (1) (2014) 11–22.
[19] S.M. Thompson, A.A. Hathaway, C.D. Smoot, C.A. Wilson, H.B. Ma, R.M. Young, L. Greenberg, B.R. Osick, S. Van Campen, B.C. Morgan, D. Sharar, N. Jankowski, Robust thermal performance of a flat-plate oscillating heat pipe during high-gravity loading, J. Heat Transfer 133 (August) (2011) 104504.
[20] L. Xiao, Y. Cao, Recent advances in pulsating heat pipes and its derivatives, J. Enhanc. Heat Transfer 19 (3) (2012) 213–231.
[21] Y. Ji, H. Chen, Y.J. Kim, Q. Yu, X. Ma, H.B. Ma, Hydrophobic surface effect on heat transfer performance in an oscillating heat pipe, J. Heat Transfer 134 (7) (2012) 74502.
[22] J. Qu, H. Wu, P. Cheng, Start-up, heat transfer and flow characteristics of silicon-based micro pulsating heat pipes, Int. J. Heat Mass Transfer 55 (21–22) (2012) 6109–6120.
[23] X. Liu, Y. Chen, M. Shi, Dynamic performance analysis on start-up of closed-loop pulsating heat pipes (CLPHPs), Int. J. Therm. Sci. 65 (2013) 224–233.
[24] S. Khandekar, N. Dollinger, M. Groll, Understanding operational regimes of closed loop pulsating heat pipes: an experimental study, Appl. Therm. Eng. 23 (2003) 707–719.
[25] X. Xue, R. Luck, B. Dawsey, J.T. Berry, Modeling of temperature measurement process with a thermocouple: a comprehensive parametric study and some experimental results, Trans. Am. Found. Soc. 112 (2004) 1–18.
[26] D. Rittel, Transient temperature measurement using embedded thermocouples, Exp. Mech. 38 (2) (1998) 73–78.
[27] B.W. Asay, S.F. Son, P.M. Dickson, L.B. Smilowitz, B.F. Henson, An investigation of the dynamic response of thermocouples in inert and reacting condensed phase energetic materials, Propel. Explos. Pyrotech. 30 (3) (2005) 199–208.
[28] J.L. Xu, X.M. Zhang, Start-up and steady thermal oscillation of a pulsating heat pipe, Heat Mass Transfer 41 (2005) 685–694.
[29] S.M. Thompson, H.B. Ma, A statistical analysis of temperature oscillations on a flat-plate oscillating heat pipe with Tesla-type check valves, Front. Heat Pipes 2 (2011).
[30] O. Suzuki, Heat-transport characteristics of a bubble-driven non-looped heat-transport device, Trans. Japan Soc. Mech. Eng. Part B 69 (678) (2003) 430–436.
[31] J.-S. Kim, N.H. Bui, H.-S. Jung, W.-H. Lee, The study on pressure oscillation and heat transfer characteristics of oscillating capillary tube heat pipe using mixed working fluid, Korean Soc. Mech. Eng. Int. J. 17 (10) (2003) 1533–1542.
[32] Y. Zhang, A. Faghri, Oscillatory flow in pulsating heat pipes with arbitrary numbers of turns, J. Thermophys. Heat Transfer 17 (3) (2003) 340–347.
[33] M. Furukawa, Rationalized concise descriptions of fluid motions in an oscillating/pulsating heat pipe, J. Heat Transfer 136 (September) (2014).
[34] H.B. Ma, B. Borgmeyer, P. Cheng, Y. Zhang, Heat transport capability in an oscillating heat pipe, J. Heat Transfer 130 (August 2008) (2008) 1–7.
[35] H.B. Ma, M.A. Hanlon, C.L. Chen, An investigation of oscillating motions in a miniature pulsating heat pipe, Microfluidics Nanofluidics 2 (2006) 171–179.
[36] M. Mameli, M. Marengo, S. Khandekar, Local heat transfer measurement and thermo-fluid characterization of a pulsating heat pipe, Int. J. Therm. Sci. 75 (2014) 140–152.
[37] S. Khandekar, M. Groll, On the definition of pulsating heat pipes: an overview, in: Proc. 5th Minsk International Seminar (Heat Pipes, Heat Pumps and Refrigerators), 2003, p. 12.
[38] A.V. Oppenheim, R.W. Schafer, Discrete-Time Signal Processing, Prentice Hall, 2009.
[39] J.S. Bendat, A.G. Piersol, Random Data: Analysis and Measurement Procedures, Wiley, 2010.
[40] P. Cheng, H. Ma, A mathematical model of an oscillating heat pipe, Heat Transfer Eng. 32 (11–12) (2011) 1037–1046.
[41] C.Y. Ho, M.W. Ackerman, K.Y. Wu, S.G. Oh, T.N. Havill, Thermal conductivity of ten selected binary alloy systems, J. Phys. Chem. Ref. Data 7 (3) (1978) 959–1177.
[42] C.D. Smoot, H.B. Ma, C.A. Wilson, L. Greenberg, Heat conduction effect on oscillating heat pipe operation, J. Therm. Sci. Eng. Appl. 3 (2011) 24501.

[43] J.G. Monroe, S.M. Thompson, Z.S. Aspin, D.L. Jacobson, D.S. Hussey, Neutron imaging of an unbalanced flat-plate oscillating heat pipe, in: 52nd Aerospace Sciences Meeting, AIAA SciTech, (AIAA 2014–0859), 2014.
[44] Q. Wu, R. Wang, X. Liu, Y. Li, R. Xu, Y. Li, A simple model used to predict the thermal performance of flat-plate closed-loop pulsating heat pipe, Appl. Mech. Mater. 316–317 (2013) 7–12.
[45] S. Khandekar, P. Charoensawan, M. Groll, P. Terdtoon, Closed loop pulsating heat pipes - Part B: Visualization and semi-empirical modeling, Appl. Therm. Eng. 23 (2003) 2021–2033.
[46] T. Katpradit, T. Wongratanaphisan, P. Terdtoon, P. Kamonpet, A. Polchai, A. Akbarzadeh, Correlation to predict heat transfer characteristics of a closed end oscillating heat pipe at critical state, Appl. Therm. Eng. 25 (2005) 2138–2151.
[47] S. Rittidech, P. Terdtoon, M. Murakami, P. Kamonpet, W. Jompakdee, Correlation to predict heat transfer characteristics of a closed-end oscillating heat pipe at normal operating condition, Appl. Therm. Eng. 23 (2003) 497–510.
[48] S. Khandekar, X. Cui, M. Groll, Thermal performance modeling of pulsating heat pipes by artificial neural network, in: Proceedings of the 12th International Heat Pipe Conference, 2002, pp. 215–219.
[49] S.M. Thompson, Z.S. Aspin, A. Elwany, N. Shamsaei, L. Bian, Additive manufacturing of heat exchangers: a case study on a multi-layered Ti-6Al-4V oscillating heat pipe, Add. Manuf. 8 (October) (2016) 163–174.
[50] J.G. Monroe, O.T. Ibrahim, S.M. Thompson, N. Shamsaei, L. Bian, A. Elwany, Thermal performance and surface characterization of a selective laser melted flat-plate oscillating heat pipe, in: Solid Freeform Fabrication Symposium 2015, 2015, p. 11.